Accepted Manuscript. Published as:

A. Picone, A. Lodesani, M. Capra, A. Brambilla, F. Bottegoni, M. Jugovac, Asish K. Kundu, P.M. Sheverdyaeva, P. Moras,

From Cr carbide to Cr oxide through a graphene layer,

Applied Surface Science, Volume 599, 2022, 153926,

ISSN 0169-4332,

https://doi.org/10.1016/j.apsusc.2022.153926.

(https://www.sciencedirect.com/science/article/pii/S0169433222014696)

From Cr carbide to Cr oxide through a graphene layer

A. Picone, A. Lodesani, M.Capra, A. Brambilla, F.Bottegoni

Dipartimento di Fisica, Politecnico di Milano,o da Vinci 32, 20133 Milano, Italy

Asish K. Kundu, P. M. Sheverdyaeva, P. Moras

Istituto di Struttura della Materia-CNR (ISM-CNR), SS 14, Km 163,5, 34149 Trieste, Italy

Interfacing graphene with ultrathin oxide films is a crucial step towards its integration in novel electronic devices. However, obtaining two-dimensional oxide films on top of graphene is a formidable task, as the extremely low surface free energy of the graphitic substrate favors the formation of oxide clusters. Here, we demonstrate that the oxidation of a Cr carbide film intercalated between graphene and a Ni(111) substrate triggers the de-intercalation of Cr atoms, which form a continuous and atomically flat Cr oxide wetting layer on top of graphene.

Microscopic and spectroscopic analyses demonstrate that the process affects marginally the structural integrity and electronic properties of graphene with respect to the pristine graphene/Ni(111) case. These findings show a new method to obtain high quality graphene/Cr oxide interfaces. In perspective, these well-defined junctions could be used to finely control the electrical conductivity of graphene through an insulating oxide gate.

Introduction

The isolation of a graphene (Gr) monolayer has boosted intense experimental and theoretical research in the field of two-dimensional (2D) materials.[1,2,3] Nowadays, stacks of different 2D materials promise the discovery of novel functional behaviors and related applications.[4,5,6] Heterostructures in which graphene is coupled with ultrathin oxide films are particularly appealing, since the dielectric character of oxides can be used to modulate the electrical conductivity of graphene. In addition, magnetoelectric or ferromagnetic oxide gates could allow for the manipulation of the spin degree of freedom,[7,8] thus paving the way towards the development of graphene-based spin field effect transistors.[9,10]

So far, only few examples of atomically flat and continuous graphene/oxide interfaces have been reported.[11,12] The main limiting factor for the growth of these systems is the low surface free energy of graphene (about 0.115 J/m^2)[13], which favors the nucleation of three-dimensional clusters. Oxide-terminated graphene/oxide heterostructures have been produced either by reactive deposition of metals in oxygen atmosphere[14,15] or oxidation of metallic materials pre-deposited on top of graphene.[16,17] Alternatively, FeO and NiO films have been stabilized below graphene by exposing Fe-intercalated Gr/Pt(111)[18] and Gr/Ni(111)[19] interfaces to high oxygen partial pressures (10^{-4}-10^{0} mbar).

Recently, we showed that reactive deposition of Cr in oxygen atmosphere on a Gr/Ni(111) substrate kept at 300 °C produces an epitaxial Cr_2O_3(0001) wetting layer with the same in-plane lattice parameter of the underlying graphene sheet.[20] Cr oxide grows on graphene in a layer-by-layer fashion up to the completion of four atomic layers. These structural properties make the Cr_2O_3(0001)/Gr/Ni junction a candidate for graphene-based electronic devices.

In this paper, we describe an alternative growth method to obtain the Cr_2O_3(0001)/Gr/Ni heterostructure. Our previous research shows that Cr intercalates below graphene, when deposited under ultra-high vacuum (UHV) conditions on Gr/Ni kept at 400 °C.[21] This process leads to the formation of an ordered Cr carbide layer between graphene and Ni, through the incorporation of C impurities dissolved in bulk Ni. Here, we demonstrate that, upon exposure to oxygen at 500 °C, Cr de-intercalates and forms an insulating Cr_2O_3(0001) layer, in analogy with the reactive deposition method. Scanning tunneling microscopy (STM) and photoelectron spectroscopy reveal a negligible effect of these processes on the structural properties and electronic states of graphene, which closely recall those of pristine Gr/Ni.

Materials and Methods

The experiments were performed in two UHV systems for microscopic and spectroscopic analysis. The Ni(111) single crystal substrate was prepared by several cycles of sputtering with 1.5 keV Ar ions and annealing at 500 °C. For graphene preparation, the clean Ni(111) surface was exposed at 500 °C to 3000 L of ethylene at a pressure of 2×10^{-5} mbar. After dosing ethylene, the sample was kept at 500 °C in UHV for 5 min. This procedure stabilizes an epitaxial graphene layer with crystallographic axes aligned to those of Ni(111). Cr was sublimated from a metallic rod heated by electron bombardment with a rate of 0.2 nm per minute, as measured by a quartz microbalance. This rate was cross-checked by evaluating the attenuation of the Ni3*p* photoemission peaks after the deposition of 1.8 nm Cr on the clean Ni substrate at room temperature [the corresponding metallic Cr3*p* line is shown in the top spectrum of Fig. 2(e)]. The intercalation of 1.2 nm Cr below graphene was performed at 400 °C. The sample was oxidized by backfilling the UHV chambers with molecular oxygen at a pressure of 1×10^{-5} mbar for 5 minutes, with the sample kept at 500 °C. Since Cr tends to dissolve in Ni with increasing the substrate temperature, the Cr content of the intercalated and oxidized samples, determined from the Cr3*p* core levels, does not scale linearly with the deposition rate. STM images in constant current mode were obtained at room temperature by an Omicron variable temperature microscope. The STM tips were formed by electrochemical etching of a tungsten wire. The photoelectron spectroscopy experiments were performed at the VUV-Photoemission beamline (Elettra, Trieste) at room temperature by a Scienta R-4000 hemispherical analyzer. Angle-resolved photoelectron spectroscopy (ARPES) data were acquired at 70 eV photon energy with energy and angular resolutions of 25 meV and 0.3°. The energy resolution for core level analysis at higher photon energies (370 and 650 eV) was set between 30 and 80 meV.

Results and discussion

The top row of Fig. 1 reports low energy electron diffraction (LEED) patterns for (a) the reference Gr/Ni system and for Cr-intercalated Gr/Ni (b) before and (c) after the exposure to molecular oxygen. The hexagonal pattern of Fig. 1(a) demonstrates that the symmetry axes of graphene are aligned to those of the substrate, in agreement with our previous results.[21,22] Rotational graphene domains, which grow on top of Ni carbide, are not visible in the LEED pattern and in the corresponding STM image [Fig. 1(d)]. They are evaluated to be in the order of 1-2% of the aligned graphene layer on the basis of the C1*s* core level analysis [Fig. 2(a)]. The deposition of 1.2 nm Cr at 400 °C induces the formation of a Moiré pattern with 8×8 super-periodicity with respect to Gr/Ni [Fig. 1(b)]. The STM image of this system [Fig. 1(e)] displays large terraces separated by steps

corresponding to the height of a Ni(111) atomic plane, i.e. 0.2 nm [line scan in Fig. 1(h)]. The inset of Fig. 1(e) shows that the Moiré super-cell is generated by a height modulation of the graphene layer in contact with the lattice-mismatched Cr carbide layer. After exposure to molecular oxygen at 500 °C, the LEED pattern of the system reverts to 1×1 [Fig. 1(c)]. The corresponding STM image [Fig. 1(f)] shows an atomically flat surface morphology, where the terraces are separated by steps slightly higher than the Ni(111) atomic plane [line scan of Fig. 1(i)] and the Moiré modulation is absent [inset of Fig. 1(f)].

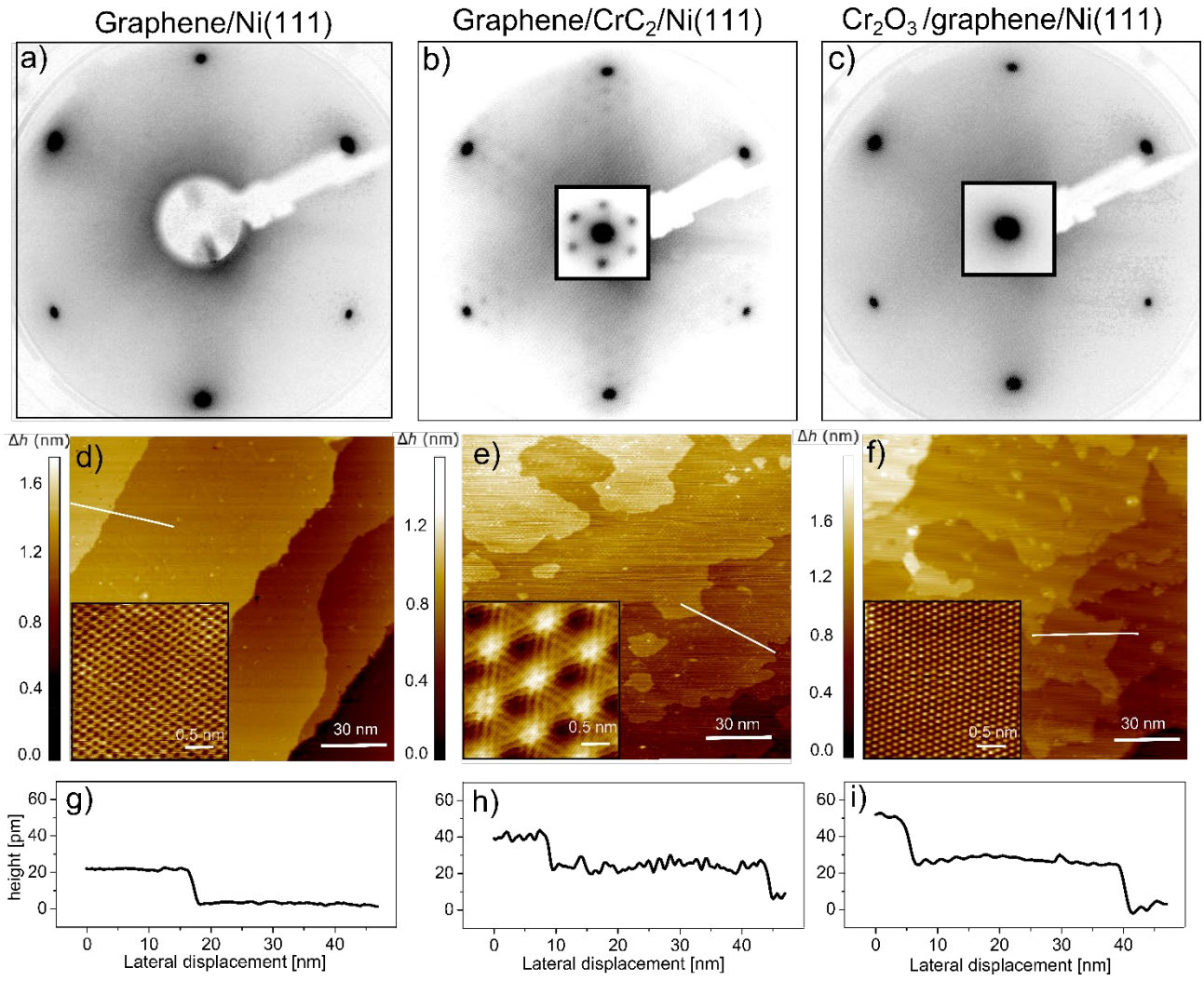

Figure 1. Top: LEED patterns acquired at 150 eV on (a) Gr/Ni, (b) 1.2 nm Cr intercalated below Gr/Ni and (c) after the oxidation of (b). The insets display the (0,0) spot measured at 45 eV. Center: STM images showing the flat surface morphology on the mesoscopic scale for the (d) Gr/Ni, (e) intercalated and (f) oxidized samples corresponding to the patterns of panels (a), (b) and (c), respectively. The insets display atomically resolved zooms of the main images. Bottom: (g,h,i) constant current scans taken along the white lines of panels (d,e,f), respectively. STM images have

been acquired at V= 1 V and I= 1 nA. STM images size is 150×150 nm^2 for panels (d), (e) and (f). The size of the insets is 5.5× 5.5 nm^2.

Fig. 2 displays core level spectra acquired at the different preparation stages.The C1*s* line of Gr/Ni [Fig. 2(a)] displays the main graphitic peak at 284.86 eV and, as anticipated in the previous paragraph, a minor component related to Ni carbide at 283.20 eV, in agreement with the literature.[23,24] Upon deposition of 1.2 nm Cr at 400 °C [Fig. 2(b)] the main peak presents the same area of the pristine case. This is a direct signature of full Cr intercalation below graphene. The graphitic peak shifts towards higher binding energy to 284.93 eV and widens with respect to Gr/Ni, as can be seen by comparing the values of full width at half maximum (FWHM) reported in the panels. These changes are a consequence of the interaction between graphene and Cr carbide. In particular, the increased FWHM of the graphitic peak is related to the presence of multiple adsorption sites with slightly different adsorption energies at the mismatched interface. The C1*s* component observed at 282.78 eV is due to the incorporation of C atoms, provided by the Ni bulk reservoir, into the Cr carbide layer. The center spectrum of Fig. 2(e) displays the Cr3*p* peak of this layer. Its binding energy (42.40 eV) is significantly lower than that of a metallic Cr layer [41.95 eV, top spectrum of Fig. 2(e)], in agreement with the trend observed in Cr carbide alloys.[25] By scaling the intensities of the Cr3*p* and carbidic C1*s* peaks for the different inelastic mean free paths and photoemission cross sections the stoichiometry of Cr carbide turns out to be approximately CrC_2, in agreement with Ref. 21. From the attenuation of the Ni3*p* peak before and after Cr intercalation [top and center spectra in Fig. 2(f)] the thickness of the Cr carbide layer is estimated of around 1.0 nm.

Once the Cr-intercalated system is exposed to molecular oxygen at 500 °C, the C1*s* peak related to Cr carbide disappears, while the binding energy and the FWHM of the graphitic component become very similar to those of the pristine Gr/Ni system [Fig. 2(c)]. Hence, the process of oxidation breaks the Cr-C bonds of the carbidic layer and restores the interface between graphene and Ni. The attenuation of the graphitic C1*s* peak is ascribed to the presence of a Cr_2O_3 layer of about 0.4 nm on top of graphene. This is demonstrated by the Cr3*p* line at 43.46 eV (bottom spectrum of Fig. 2(e)) and the appearance of the O1s peak at 530.25 eV [Fig. 2(g)], in agreement with spectroscopic data for the Cr_2O_3/Cu(111) interface.[26] It is worth noting that the intensity of the Cr3*p* peak decreases upon oxidation [Fig. 2(e)], despite Cr oxide lies on the surface and Cr carbide is intercalated below graphene. This is a consequence of the thermal treatment during the oxidation procedure: the employed temperature (500 °C) promotes the interdiffusion of a fraction of the Cr atoms into the Ni substrate, thus resulting in a lower Cr content in the near surface region. The C1*s* peak of Fig. 2(c) presents a component at 284.25 eV, which is not observed in Fig. 2(a,b) and the lineshape of the

corresponding Ni3*p* core level (bottom spectrum of Fig. 2(f)) is much less defined than before oxidation. These features can be linked to the formation of NiO at the interface between graphene and Ni, by comparison with spectroscopic results for oxidized Gr/Ni.[19] At variance with that case, the NiO content is so small that no decoupling effect is seen on the graphene valence band [see Fig. 3(c,d)].

Fig. 2(d) reports C1*s* spectra for the reactive growth of 0.3 and 0.6 nm of Cr_2O_3 on Gr/Ni. The graphitic peaks and the component related to NiO are analogous to those detected in Fig. 2(c), although their relative ratio changes in favor of the second component with increasing the thickness of the Cr oxide layer. This observation can be associated to the duration of the reactive growth, during which oxygen can penetrate below the protective graphene layer. Besides NiO formation, that can be most likely controlled by varying the growth parameters, the two growth methods appear to produce equivalent systems, as also demonstrated by the following valence band analysis.

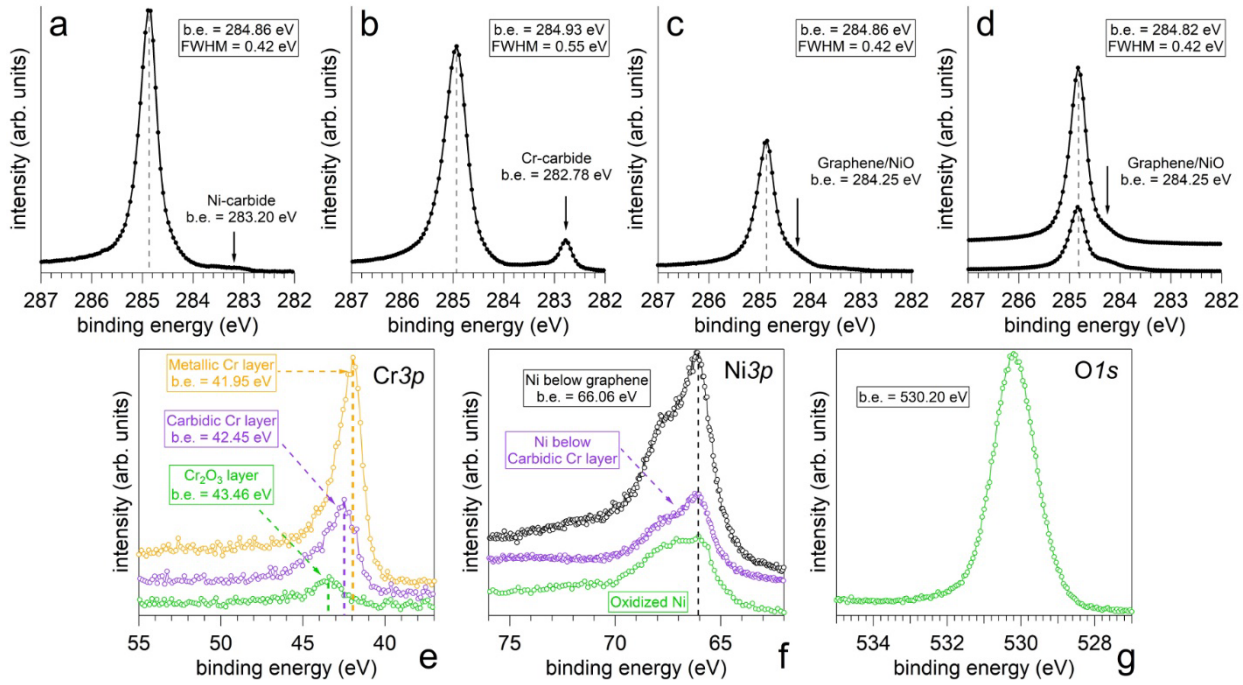

Figure 2: C1*s* spectra for (a) Gr/Ni, Cr intercalated below Gr/Ni (b) before and (c) after oxidation and (d) reactive deposition of 0.6 and 1.2 nm Cr on Gr/Ni. Binding energy and FWHM of the graphitic peaks are reported in the boxes. The intensity axis of panels (a-d) is absolute to ease the comparison. (e) Cr3*p* spectra for metallic Cr (top), Cr carbide (center) and Cr oxide (bottom) Cr. The metallic Cr spectrum has been acquired after deposition of Cr on Gr/Ni at room temperature, where Cr does not intercalate underneath graphene. (f) Ni3*p* spectra corresponding to the sequence of panels (a-c) from top to bottom. C1*s*, Cr3*p* and Ni3*p* spectra are measured with photon energy 370 eV. (g) O*1s* spectrum of the Cr oxide layer. Photon energy 650 eV.

Fig. 3 shows ARPES data taken along the Γ-K direction of graphene, which is aligned with the $\overline{\Gamma}$-$\overline{K}$ axis of Ni(111), for the systems discussed in Fig. 2. In all cases, the π and σ bands can be clearly identified. The energy position of the π and σ band bottom at Γ and K, respectively, and that of the Dirac point at K are marked by open circles and summarized in Table I. A precise determination of the Dirac points, which are very close to the onset of intense Ni3*d* and/or Cr3*d* bands, is derived from Fig. 4.

The dispersion of the graphene bands of Gr/Ni (Fig. 3(a)) agrees well with the ARPES data published in the literature.[27, 30, a,b] After Cr intercalation (Fig 3(b)) the bottom of the π and σ bands shift upward by 0.4 and 0.1 eV with respect to Gr/Ni.. Dispersive features near the Fermi level are generated by overlapping Ni3*d* and Cr3*d* states. The black arrows around $k_{||}$ = 1.0 Å^{-1} indicate one band that can be assigned to the ordered Cr carbide layer. The oxidation process restores the interface between graphene and Ni, i.e. removes bands related to Cr carbide and shifts the bottom of the π and σ bands to the original position [Fig. 3(c)]. The formation of Cr oxide on top of graphene manifests with a reduction of the intensity of graphene and Ni bands, the appearance of O-derived states between 3.5 and 8 eV and the shift of the Cr3*d* states to 2.2 eV. Similar electronic features are seen on the sample prepared by reactive deposition [Fig. 3(d)]. In this case, the insulating character of the Cr oxide layer is indicated more clearly by the drop of the photoemission signal near the Fermi level.

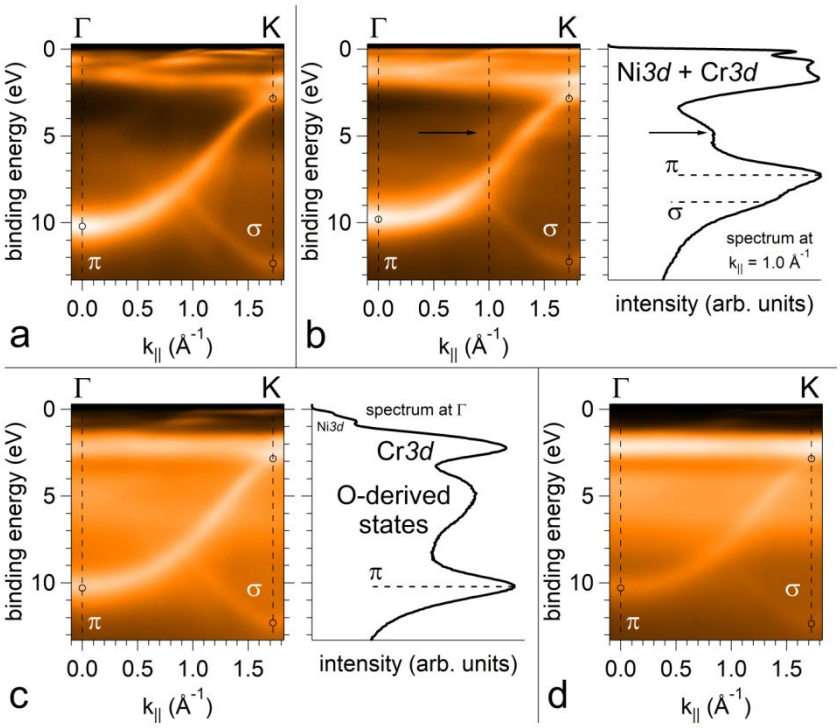

Figure 3: ARPES spectra for (a) Gr/Ni, Cr intercalated below Gr/Ni (b) before and (c) after oxidation of 1.2 nm Cr on Gr/Ni and for (d) 0.6 nm Cr_2O_3 layer grown by reactive deposition on Gr/Ni. In panel

(b) black arrows indicate the presence of a feature related to the ordered Cr carbide layer. In panel (c) the spectrum extracted at Γ shows the prominent Cr and O states.

Table I. Energy position of the π and σ band bottom and of the Dirac point derived from Figs. 3 and 4.

Energies in eV	π band at Γ	σ band at K	Dirac point at K
Gr/Ni	10.20	12.35	2.85
Cr-intercalated Gr/Ni	9.80	12.25	2.85
Cr_2O_3/Gr/Ni	10.30	12.30	2.85
Reactive deposition	10.30	12.35	2.85

The region near the Fermi level of systems displayed in Fig. 3(a-c) can be better visualized in Fig. 4. Here, the ARPES signal is collected along arcs of a circle centered at Γ and with radius 1.72 $Å^{-1}$, which cut the electronic structure of graphene through its K points. The direct spectra and their first derivatives (along the energy axis) are reported on the left and right column of the figure, respectively. The dispersion of the graphene π states of the Gr/Ni system (Fig. 4(a)) is very similar to that observed in Ref. [27]. Two linearly dispersing bands (labeled with π in the figure) cross at 2.85 eV in correspondence with the K point. Within our energy resolution, there is no evidence of a gap opening at their crossing, which is identified with the Dirac point of a Dirac cone. The slope of the bands above and below the Dirac point (highlighted by white dots in the first derivative data) is different. The hybridization with the Ni3*d* states is responsible of the flatter dispersion of the upper part of the π state and its suppression for binding energies lower than 2.55 eV in full agreement with Ref. 27. Cr intercalation results mainly in the formation of a Cr-related band at the Fermi level, while the Dirac cones present the same properties of the pristine case [Fig. 4(b)]. Also the formation of Cr oxide on top of graphene has negligible effects on its Dirac cones [Fig. 4(c)].

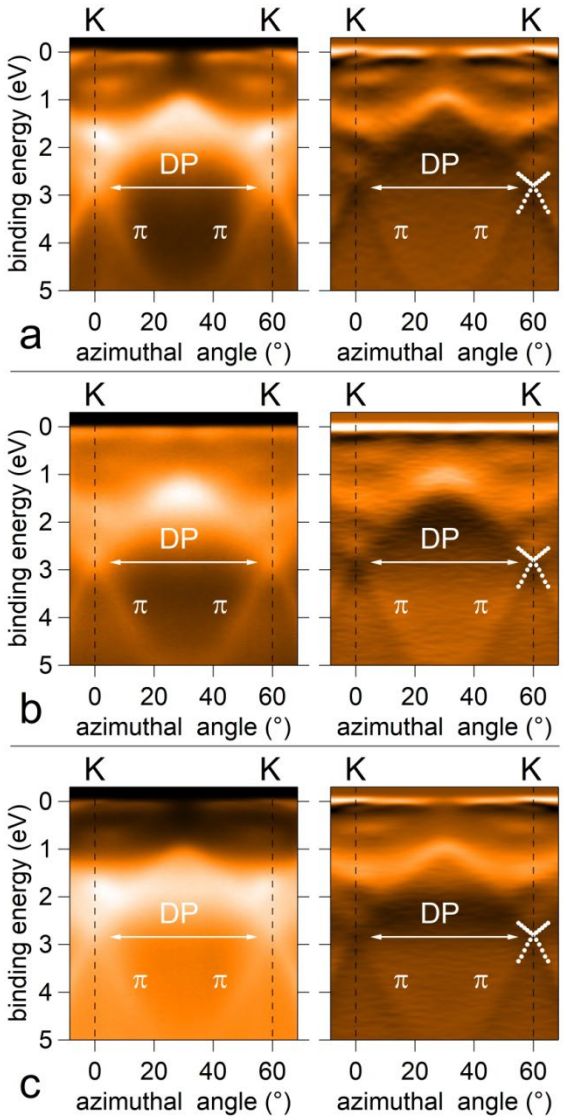

Figure 4: ARPES spectra for (a) Gr/Ni, 1.2 nm Cr intercalated below Gr/Ni (b) before and (c) after oxidation, taken along arcs of the circle centered at Γ and passing though the K points of graphene. The right column displays the raw data of the left column in the first derivative form to enhance the sensitivity to the relatively weak π bands. White dots indicate the dispersion of the π bands near the Dirac point.

The STM measurements of Fig. 1 (see also supplementary information for further STM measurements) and the spectroscopic data of Fig. 1-3 support the formation of a flat Cr_2O_3(0001) wetting layer on top of Gr/Ni, in close analogy with the case of reactive growth.[20]

Cr is able to cross the graphene barrier in both directions while keeping the 2D morphology of the original Gr/Ni system over mesoscopic areas, as demonstrated by STM. The intercalated and de-intercalated systems present well defined graphene bands, whose dispersion appears to be determined by the strong interaction with the substrate. The epitaxial Cr_2O_3 layer at the surface has a

clear insulating character from the first few atomic layers, which make it potentially suitable for future applications.

The observation of an atomically flat and homogeneous oxide layer on top of graphene deserves further discussion. Generally, the interface and surface energy balance trigger the formation of three-dimensional oxide clusters on graphene. The surface free energy of the bulk terminated $Cr_2O_3(0001)$ is very large[28] (3.1 J/m^2) as compared to that of graphene,[13] therefore the observed flat morphology implies that the metal-rich oxygen termination discussed in Refs 20 and 29 (see also supplementary information) lowers drastically the surface free energy of the oxide. The uniformity of the oxide layer suggests that Cr de-intercalation is not limited to defective regions of graphene, as reported for the oxidation of similar intercalated systems,[30] but involves the whole sheet.

A mechanism compatible with the observed Cr de-intercalation process is suggested in Ref. 31. The intercalation of Si atoms between graphene and Ru(0001) is facilitated by the formation of C vacancies in the honeycomb lattice, induced by the cooperation of Si and Ru atoms. After the intercalation, the vacancies are repaired by C atoms dissolved in the substrate. Similarly, in the present case the synergic action of Cr atoms and oxygen molecules could create C vacancies, which are repaired by C atoms provided by the Cr carbide layer.

It is interesting to notice that the oxidation of ultrathin films intercalated underneath graphene generally leads to an oxidized layer at the interface between graphene and the substrate [see 19 amd 18 and S. Lizzit et al. Nano Lett. 12, 4503 (2012), and H. Guo et al. Nano Lett. 20, 8584 (2020)], while in our case the oxide film develops on top of the graphitic layer. Besides the thermodynamic explanation based on the low surface free energy of the peculiar metal-rich termination of Cr2O3(0001) discussed above, also the kinetics of the metal oxidation can play a role. Generally, the oxide thickening takes place either by the penetration of oxygen inside the metal or the migration of metal atoms on top of the oxide surface. In the case of Cr2O3, it is found that the oxide film grows preferentially through the migration of Cr cations on the top of the surface (G. Salomonsen, N. Norman, O. Lønsjø, T.G. Finstad Kinetics and mechanism of oxide formation on titanium, vanadium and chromium thin films J. Less Common Met., 158 (2) (1990), pp. 251-26). Therefore, it is reasonable that the oxidation of the intercalated CrC_2 film leads to the de-intercalation of Cr.

Conclusions

Cr intercalation at the Gr/Ni interface gives rise to an ultrathin Cr carbide layer, which strongly affects the electronic structure of graphene, similarly to Ni. The oxidation at relatively low pressure of molecular oxygen restores the interface between graphene and Ni and promotes the de-

intercalation of Cr, which forms a homogeneous Cr_2O_3 layer on top of graphene. The ordered de-intercalation does not damage the carbon monolayer, indicating that atoms can segregate on the surface through a complete layer of graphene. A cooperative mechanism for the Cr mass transport through the formation and annihilation of C vacancies is suggested.

Acknowledgements

We acknowledge the project EUROFEL-ROADMAP ESFRI

References

1. K.S. Novoselov, A.K. Geim, S.V.Morozov Electric field effect in atomically thin carbon films. *Science* **2004** , *306* ,666–669.
2. Castro Neto, A H Guinea, F. Peres, N. M. R. Novoselov, K. S. and A. K. Geim The electronic properties of graphene. *Rev. Mod. Phys*. **2009**, *81*,109–62.
3. Zhu, Y. Murali, S. Cai, W. Li, X. Suk, J.W. Potts, J.R. and R. S. Ruoff Graphene and graphene oxide: synthesis, properties, and applications. *Adv. Mater.* **2010**, *22***,** 3906–24.
4. Geim A and Grigorieva I Van der Waals heterostructures. *Nature* **2013**, *499*, 419–25.
5. Novoselov K S, Mishchenko A, Carvalho A and Castro Neto A H 2D materials and van der Waals heterostructures. *Science* **2016,** *353*, 943.
6. Britnell, L Gorbachev, R. V. Jalil, R. Belle, B. D. Schedin, F. Mishchenko, A. Georgiou, T. Katsnelson, M. I. Eaves, L. Morozov, S. V. Peres, N. M. R. Leist, J. Geim, A. K. Novoselov, K. S and L. A. Ponomarenko Field-effect tunneling transistor based on vertical graphene heterostructures. *Science* **2012**, *335***,** 947–50.
7. Wei, P. Lee, S. Lemaitre, F. Pinel, L. Cutaia, D. Cha, W. Katmis, F. Zhu, Y Heiman, D. Hone, J Moodera, J.S. and Ching-Tzu Chen Strong interfacial exchange field in the graphene/EuS heterostructure. *Nature Materials* **2016**, *15*, 711.
8. R. Choudhary, R. Skomski, A. Kashyap Electric-field control of magnetism in graphene on chromia. *J. Magn. Magn. Mater.* **2017**, *443***,** 4-8.
9. Semenov Y.G, Kim K.W., Zavada J.M Spin field effect transistor with a graphene channel. *Appl. Phys. Lett.* **2007**, *91*, 153105.
10. Popinciuc, M.; Józsa, C.; Zomer, P.; Tombros, N.; Veligura, A.; Jonkman, H.; Van Wees, B. Electronic Spin Transport in Graphene Field-Effect Transistors. *Phys. Rev. B: Condens. Matter Mater. Phys.* **2009**, *80***,** 214427.
11. Addou, R.; Dahal, A.; Batzill, M. Growth of a Two-Dimensional Dielectric Monolayer on Quasi-Freestanding Graphene. *Nat. Nanotechnol*. **2013**, *8***,** 41−45.
12. L. Omiciuolo, E. R. H. a. ndez, E. Miniussi, F. Orlando, P. Lacovig, S. Lizzit, T. O. M.scedil, A. Locatelli, R. Larciprete, M. Bianchi, S. Ulstrup, P. Hofmann, D. Alf_e, A. Baraldi Bottom-up approach for the low-cost synthesis of graphene-alumina nanosheet interfaces using bimetallic alloys. *Nat. Commun.* **2014**, *5***,** 5062.
13. Van Engers, C. D.; Cousens, N. E.; Babenko, V.; Britton, J.; Zappone, B.; Grobert, N.; Perkin, S. Direct Measurement of the Surface Energy of Graphene. *Nano Lett.* **2017**, *17*, 3815−3821.

14. Novotny, Z.; Netzer, F. P.; Dohnálek, Z. Cerium Oxide Nanoclusters on Graphene/Ru(0001): Intercalation of Oxygen via Spillover. ACS Nano **2015**, *9*, 8617−8626.
15. Ryan T. Frederick, Zbynek Novotny, Falko P. Netzer, Gregory S. Herman and Zdenek Dohnále Growth and Stability of Titanium Dioxide Nanoclusters on Graphene/Ru(0001). *J.Phys.Chem.B* **2018**, *122*, 640−648.
16. Y.S. Dedkov, A. Generalov, E. Voloshina and M. Fonin Structural and electronic properties of Fe_3O_4/graphene/Ni(111) junctions. *Phys. Status Solidi RRL* **2011**, *5*, 226-228.
17. Rodrigo Cezar de Campos Ferreira, Luis Henrique de Lima, Lucas Barreto, Caio C. Silva, Richard Landers and Abner de Siervo Unraveling the Atomic Structure of Fe Intercalated under Graphene on Ir(111): A Multitechnique Approach. *Chem. Mater.* **2018**, *30*, 7201−7210.
18. Dahal, A. Batzill, M. Growth from Behind: Intercalation-Growth of Two-Dimensional FeO Moiré Structure Underneath of Metal-Supported Graphene. *Sci. Rep*. **2015**, *5*,11378.
19. Dedkov, Y. Klesse, W. Becker, A. Späth, F. Papp, C. Voloshina, E. Decoupling of Graphene from Ni(111) via Formation of an Interfacial NiO Layer. *Carbon* **2017**, *121*, 10−16.
20. Lodesani, A. Picone, A. Brambilla, A. Giannotti, D. Jagadeesh, M. Calloni, A. Bussetti, G. Berti, G. Zani, M. Finazzi, M. Duò, L. and Ciccacci F. Graphene as an Ideal Buffer Layer for the Growth of High-Quality Ultrathin Cr_2O_3 Layers on Ni(111). *ACS Nano* **2019**, *13*, 4361-4367
21. Picone, A.; Giannotti, D.; Finazzi, M.; Duò, L.; Ciccacci, F.; Brambilla, A. Intercalation from the Depths: Growth of a Metastable Chromium Carbide between Epitaxial Graphene and Ni(111) by Carbon Segregation from the Bulk. *J. Phys. Chem. C* **2017**, *121,* 16803−16809.
22. M. S. Jagadeesh, A. Calloni , G. Bussetti , L. Duò and F. Ciccacci Spin-Resolved PES and IPES Investigation of the Graphene/Ni(111) Interface. *Phys. Status Solidi B* **2017**, *255*, 1700415.
23. Patera, L. L. Africh, C. Weatherup, R.S. Blume, R. Bhardwaj, S. Castellarin-Cudia, C. Knop-Gericke, A. Schloegl, R. Comelli, G. Hofmann, S. and C. Cepek In Situ Observations of the Atomistic Mechanisms of Ni Catalyzed Low Temperature Graphene Growth. *ACS Nano* **2013**, *7*, 7901.
24. Africh, C. Cepek, C. Patera, L. L. Zamborlini, G. Genoni, P. Menteş, T. O. Sala, A. Locatelli, A. and G. Comelli Switchable graphene-substrate coupling through formation/dissolution of an intercalated Ni-carbide layer. *Sci. Rep.* **2016**, *6*, 19734.

25. M. Detroye, F. Reniers, C. Buess-Herman, and J. Vereecken AES–XPS study of chromium carbides and chromium iron carbides *Appl. Surf. Sci.* **1999**, *144-145* 78.
26. J. Pantförder, R. Domnick, Ch. Ammon, G. Held, and H.-P. Steinrück Formation of a new type of chromium oxide by deposition of chromium onto water precovered Cu(111) S*urf. Sci.* **2001**, *480***,** 73.
27. A. Varykhalov, D. Marchenko, J. Sánchez-Barriga, M. R. Scholz, B. Verberck, B. Trauzettel, T. O. Wehling, C. Carbone, and O. Rader Intact Dirac Cones at Broken Sublattice Symmetry: Photoemission Study of Graphene on Ni and Co *Phys. Rev. X* **2012**, *2*, 041017.
28. C.Rehbein, N.M.Harrison, A.Wander Structure of the a-Cr_2O_3 (0001) surface: An ab initio total-energy study. *Phys.Rev.B* **1996**, *54*, 14066–14070.
29. Kramer, A.; Bignardi, L.; Lacovig, P.; Lizzit, S.; Batzill, M. Comparison of Surface Structures of Corundum Cr_2O_3 (0001) and V_2O_3 (0001) Ultrathin Films by X-Ray Photoelectron Diffraction. J. Phys.: Condens. Matter **2018**, *30*, 074002.
30. E. N. Voloshina, A, Generalov, M. Weser, S. Böttcher, K. Horn, Y. S. and Dedkov, Structural and Electronic Properties of the Graphene/Al/Ni(111) Intercalation System. *New J. Phys.* **2011**, *13***,** 113028.
31. G. Li , H. T. Zhou , L. D. Pan , Y. Zhang , L. Huang , W. Y. Xu , S. X. Du , M. Ouyang , A. C. Ferrari and H. J. Gao , J. Am. Chem. Soc., 2015, 137 , 7099 —7103.

a: Y. S. Dedkov and M. Fonin, Electronic and magnetic properties of the graphene–ferromagnet interface, 2010 *New J. Phys.* **12** 125004

b: E. Voloshina and Y. Dedkov, Graphene on metallic surfaces: problems and perspectives, Phys. Chem. Chem. Phys., 2012,14, 13502-13514